ЖЭТФ, 2002, том 122, вып. 1 (7), стр. 33–48

SCANNING OF THE $e^+e^- \to \pi^+\pi^-$ CROSS-SECTION BELOW 1 GeV AT DAΦNE BY RADIATIVE EVENTS

M. I. Konchatnij, N. P. Merenkov*

National Science Centre «Kharkov Institute of Physics and Technology»
61108, Kharkov, Ukraine

Submitted 21 February 2002

The tagged photon events for the measurement of the $e^+e^- \to \pi^+\pi^-$ total cross-section by the radiative return method at DAΦNE is discussed. The effects caused by the not exactly head-on collision of beams and by the QED radiative corrections are investigated. The essential part consists of the analysis of the event selection rules that ensure the rejection of the 3-pion hadronic state and take the main properties of the multiple purpose KLOE detector into account. The study of the non-head-on effect is performed in the Born approximation by integrating over the tagged photon angles, whereas the radiative corrections are calculated neglecting this effect. Together with the quasireal electron approach, this allows us to derive analytical formulas for the correction to the cross-section of the initial-state radiative process. Some numerical calculations illustrate our analytical results.

PACS: 12.20.-m, 13.40.-f, 13.60.-Hb, 13.88.+e

1. INTRODUCTION

The recent measurement of the muon anomalous magnetic moment $a_\mu = (g-2)_\mu/2$ performed in the Brookhaven E861 experiment with the electroweak precision [1] has boosted the interest in a renewed theoretical calculation of this quantity [2]. The reported new world average has shown the discrepancy of 2.6 standard deviations with respect to the theoretical value based on the Standard Model calculation [3], and this may open a window into possible new physics beyond the Standard Model. On the other hand, the conclusion about a significant discrepancy between the reported data and the Standard Model prediction may be somewhat premature.

Theoretical estimations of a_μ include several contributions involving the nonperturbative hadronic sector of the Standard Model: vacuum polarization, light-by-light scattering, and higher-order electroweak corrections. Hadronic effects in the two-loop electroweak contribution are small, of the order of the experimental error, and the associated theoretical uncertainty can be brought under safe control [4].

The situation with hadronic effects in the light-by-light scattering radically changed in recent months (after the E861 data were reported) due to works cited in Ref. [5]. In these works, the authors used the description of the $\pi^0\gamma^*\gamma^*$ transition formfactor based on a large-N_C expansion and short-distance properties of QCD to calculate the pseudoscalar channel contribution (in the $\gamma^*\gamma^*$ system). The corresponding result disagrees by only its overall sign with the latest previous calculations of two different groups [6, 7]. It is interesting to note that the result in Ref. [5] forced both these groups to carefully check their programs, and they recently found their own (different) sources of the wrong sign for the pseudoscalar channel [8, 9].

The main ingredient of the theoretical prediction of a_μ, which is responsible for the bulk of the theoretical error, is the contribution of the hadron vacuum polarization. The problem is that it cannot be computed analytically because perturbative QCD loses its prediction power at low and intermediate energies, where on the other hand, the corresponding effect is maximum. But this contribution can be calculated from the data on the total hadronic cross-section σ_h for the process $e^+e^- \to$ hadrons using a dispersion relation [10]. Because the existing data about σ_h come from different sources and do not always meet the required accuracy, they are supplemented with a theoretical in-

*E-mail: merenkov@kipt.kharkov.ua

put. Therefore, different estimations give different results, which either strengthen the difference between theoretical and experimental values of a_μ or make it only marginal [11–14].

The cross-section σ_h also plays an important role in the evolution of the running electromagnetic coupling α_{QED} from low to high energies. This means that the interpretation of measurements at high-energy electron–positron and electron–proton colliders depends on the precise knowledge of σ_h, with one percent accuracy or even better.

The updated hadronic light-by-light contribution [5, 8, 9] decreases the discrepancy between the theory and the experiment for a_μ to 1.5 standard deviations, and the disagreement between the Standard Model and the reported experimental value becomes not so sharp. Nevertheless, when the full set of data at the BNL collaboration is analyzed, the experimental error bars are expected to decrease by the additional factor three at least, and this challenges a new test of the Standard Model. The high-precision data about σ_h will play the key role in this test.

We note that the data recently derived in the direct scanning of σ_h by CMD-2 [15] and BES II [16] collaborations were included in a new analysis [17]. This significantly reduces the error in the hadronic contribution to the shift of α_{QED} but does not remove the discrepancy in a_μ. Therefore, there exists an eminent physical reason for new measurements to accumulate high-precision data about σ_h at the total center-of-mass frame energies below 1 GeV.

The old idea to use the initial-state radiative events in the electron–positron annihilation process

$$e^-(p_1) + e^+(p_2) \to \gamma(k) + \text{hadrons}(q) \qquad (1)$$

for the scanning of the total hadronic cross-section σ_h has become quite attractive recently [18–22]. This radiative return approach allows performing the scanning measurements at the accelerators running at a fixed energy, and this circumstance is the main advantage compared to the traditional direct scanning. The reason is that the most important physical parameters, the luminosity and the beam energy, remain the same during the entire scanning at fixed-energy colliders. They must therefore be determined only once, which can be done with a very high accuracy. The drawback is of course a loss in the event number, and it is obvious that only high-luminosity accelerators can be competitive when the radiative return method is used.

It is a general opinion that the high-luminosity DAΦNE machine operating in the Φ resonance region with multiple-purpose detector KLOE is the ideal collider to scan $\sigma_h(q^2)$ with the center-of-mass energy $\sqrt{q^2}$ varying from the threshold to 1 GeV just by radiative events. It is now well understood that in this energy region, the total hadronic cross-section is mainly fulfilled by the contribution of the ρ resonance. This in turn implies that the dominant hadronic final state is that of the charged pion pair $\pi^+\pi^-$, and the KLOE detector allows measuring both the photon energy deposited in calorimeters and the 3-momenta of pions running through the drift chamber [20, 23].

Such a wide range of experimental possibilities of the KLOE detector can provide a realization of two approaches to scanning the $\pi^+\pi^-$ channel contribution to $\sigma_h(q^2)$: with tagged photon events [19, 20, 22] and without photon tagging [22, 24, 25]. The last method has some advantages because it allows including the events with collinear initial-state radiative photons, which leads to the increase of the cross-section by the energy logarithm enhancement factor [26].

On the other hand, the first data about the traditional tagged photon scanning of $\sigma_h(q^2)$ at DAΦNE are reported [26] (we also note that large radiative event rates were observed by the BaBar Collaboration [27]). To extract $\sigma_h(q^2)$ at different squared di-pion invarinat masses with one per cent accuracy, one must precisely analyze the initial-state radiative events and take the final-state radiative events and the initial-state radiative interference as a background. Moreover, the radiative corrections must be calculated for all these contributions [21]. For a realistic experimental event selection, this task can usually be solved by means of Monte Carlo event generators. But for some ideal conditions, analytical calculations may be performed with high accuracy, and this is a very important test of the required one percent accuracy produced by the Monte Carlo generators.

The high-precision analysis of the initial-state radiative events is the main attribute of the radiative return method. The corresponding radiation corrections were considered in a number of papers by both the Monte Carlo generators [19, 22] and analytical calculations [18, 22, 24]. In present paper, we derive analytical formulas for different contributions to the initial-state radiative cross-section including the first-order radiative corrections. We use the same rules for the event selection as given in [24]. These selection rules are maximum draw near the experimental ones [20, 23] except the di-pion angular phase space, for which we use the entire 4π opening angle. This is not the case with the realistic measurements at DAΦNE because there exists a so-called blind zone in the KLOE detector with

the opening angle about 15° along the electron and positron beam directions. Any particle inside this blind zone cannot be detected either by the KLOE calorimeters or by the KLOE drift chamber.

In Sec. 2, we briefly recall the selection rules used here and analyze the Born cross-section by numerically integrating the sufficiently complicated analytical formulas given in [24], which take the non-head-on beam collision into account. In Sec. 3, the contributions to radiative corrections due to the virtual and soft photon emission are obtained by analytically integrating over the angular phase space of the photon that deposits its energy in calorimeters. In Sec. 4, the effect of an additional hard photon emission inside the blind zone is investigated and the corresponding contribution to radiative corrections is derived. To perform the analytical calculation, we use the quasireal electron approximation [28] for both the differential cross-section and underlying kinematics. In Sec. 5, the total radiative correction is derived and some numerical estimates are given. The elimination of the auxiliary infrared parameter is demonstrated and the dependence of the radiative corrections to the initial-state radiative cross-section on the squared di-pion invariant mass q^2 and physical parameters defining the selection rules is investigated. We briefly summarize our results in Conclusion. In the Appendices, we give some formulas that are useful in our intermediate calculations.

2. SELECTION RULES AND THE INITIAL-STATE BORN RADIATIVE CROSS-SECTION

As mentioned above, the multiple purpose KLOE detector allows independently measuring the photon energy with two calorimeters QCAL and EMCAL and the 3-momenta of the charged pions with the drift chamber. The selection rules that we consider here can be formulated as follows: any event is included if only one hard photon with the energy $\omega > \omega_m$, $\omega_m = 50$ MeV, hits the calorimeters and if the difference between the lost energy Ω and the lost 3-momentum modulus $|\mathbf{K}|$ does not exceed a small value ηE, $\eta \ll 1$, where E is the beam energy. The lost energy is defined as the difference between the total initial energy and the sum of the charged pion energies, and the lost 3-momentum is defined similarly.

The first rule implies that in addition to one hard photon, only soft photons that cannot be recorded by the KLOE detector can hit the calorimeters. The radiation of the additional hard photon is allowed inside the blind zone. The second rule ensures the removal of the 3-pion hadronic state arising due to possible $\Phi \to \pi^+\pi^-\pi^0$ and $\omega \to \pi^+\pi^-\pi^0$ decays. The neutral pion quickly decays into two γ quanta; one of these has time to light in the calorimeters, whereas the other can fly away into the blind zone. It is easy to see that this rule does not allow the lost invariant mass to be greater than $2E^2\eta$, and the 3-pion state is therefore forbidden if $\eta < 0.035$. Thus, the following event selection cuts are imposed [20]:

$$\begin{aligned} &\Omega - |\mathbf{K}| \le \eta E, \quad \omega > \omega_m, \\ &\eta = 0.02, \quad \omega_m = 50 \text{ MeV}. \end{aligned} \tag{2}$$

The first inequality in (2) is important in calculating the contribution caused by the emission of two hard photons (one inside the calorimeters and the other in the blind zone) because it only affects the phase space of two hard photons. At the Born level (with only one photon inside the calorimeters), we must therefore take the second restriction in (2) into account by introduction the trivial Θ function. The differential distribution over the di-pion invariant mass can be written as [24]

$$\frac{d\sigma^B}{dq^2} = \frac{\alpha}{2\pi^2}\sigma(q^2)\frac{(S-q^2)d\cos\theta d\varphi}{4S(2E - |\mathbf{P}_\Phi|\sin\theta\cos\varphi)^2} \times \\ \times \frac{(S+T_1)^2 + (S+T_2)^2}{T_1T_2}\Theta(\omega - \omega_m), \tag{3}$$

$$\omega = \frac{S-q^2}{2(2E - |\mathbf{P}_\Phi|\sin\theta\cos\varphi)},$$

where θ and $\varphi(\omega)$ are the polar and azimuthal angles (energy) of the photon detected by the KLOE calorimeters. The approximation used here is valid if $E^2\theta_0^2 \gg m^2$, where $2\theta_0$ is the opening angle of the blind zone and m is the electron mass. The cross-section $\sigma(q^2)$ of the process $e^+e^- \to \pi^+\pi^-$ is expressed through the pion electromagnetic formfactor $F_\pi(q^2)$ as

$$\sigma(q^2) = \frac{\pi\alpha^2|F_\pi(q^2)|^2}{3q^2}\left(1 - \frac{4m_\pi^2}{q^2}\right)^{3/2},$$

where m_π is the pion mass. The invariants entering Eq. (3) are given by

$$T_1 = -2p_1k = -\omega\left(2E - 2P_z\cos\theta - |\mathbf{P}_\Phi|\sin\theta\cos\varphi\right),$$

$$P_z = E\left(1 - \frac{|\mathbf{P}_\Phi|^2}{8E^2}\right),$$

$$T_2 = -2p_2k = -\omega\left(2E + 2P_z\cos\theta - |\mathbf{P}_\Phi|\sin\theta\cos\varphi\right),$$

$$S = 2p_1p_2 = 4E^2 - |\mathbf{P}_\Phi|^2, \quad q^2 = S + T_1 + T_2.$$

In writing these expressions, we took into account that at DAΦNE, the electron and positron beams exercise not exactly a head-on collision at the interaction

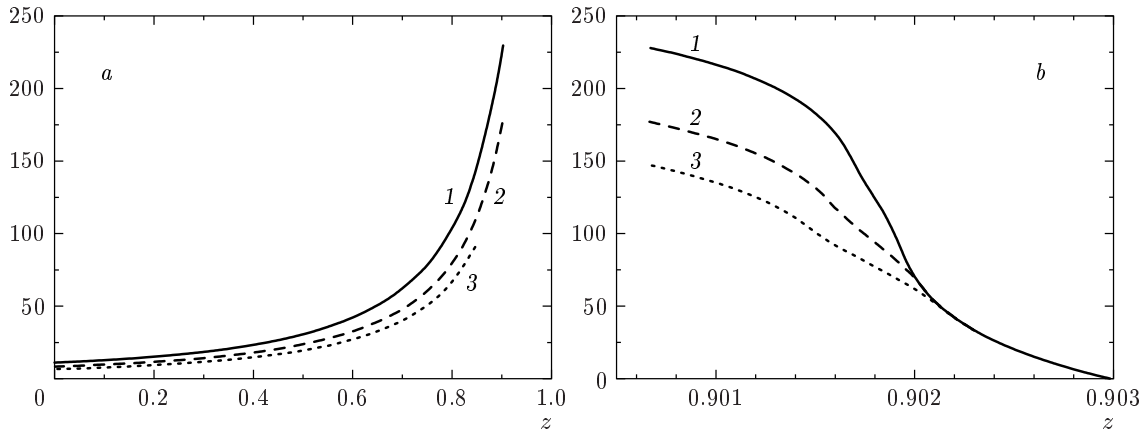

Fig. 1. The Born cross-section $\frac{d\sigma}{dz}/\left[\frac{\alpha}{2\pi}\sigma(q^2)\right]$ of the initial-state radiative process $e^+e^- \to \gamma + \pi^+\pi^-$ at different limiting angles of the blind zone versus variable z. Figure 1a corresponds to the contribution of the region $D > 1$ defined by Eq. (4). The sum of contributions of the regions $1 > D > s_0$ and $s_0 > D > -1$ is shown in Fig. 1b (see Ref. [24], Eqs. (19)–(21), for the corresponding analytical formulas). It depends on the minimum energy of the tagged photon ω_m, which we choose as 50 MeV. $\theta_0 = 5^\circ$ (*1*), 10° (*2*), 15° (*3*)

point, but there exists a small crossing angle between them that is equal to $|\mathbf{P}_\Phi|/E$, where $|\mathbf{P}_\Phi| = 12.5$ MeV. Because of a nonzero crossing angle, the energy of the tagged photon becomes dependent on its angular position, which complicates the exact analytical calculations. Thus, the question arises as to the magnitude of the corresponding effect. As shown in [24], there exist three regions,

$$D > 1, \quad 1 > D > \sin\theta_0, \quad \sin\theta_0 > D > -1,$$

where

$$D = \frac{4E(E-\omega_m) - q^2 - |\mathbf{P}_\Phi|^2}{2\omega_m |\mathbf{P}_\Phi|},$$

and the form of the initial-state radiative cross-section is different in each region. The analytical expressions for the distribution over the di-pion invariant mass is simple in the first two regions, but it seems that only a numerical integration with respect to the photon polar angle is possible in the third region. We also note that in the limiting case as $|\mathbf{P}_\Phi| \to 0$, only the first region can occur with the obvious restriction

$$4E(E-\omega_m) > q^2.$$

The results of our calculations of the Born cross-section are shown in Figs. 1 and 2. It follows from Fig. 1 that the contribution of the first region ($D > 1$) dominates in a wide interval of the di-pion invariant masses. Within the approximation

$$4E^2(1-c_0) \gg \mathbf{P}_\Phi^2,$$

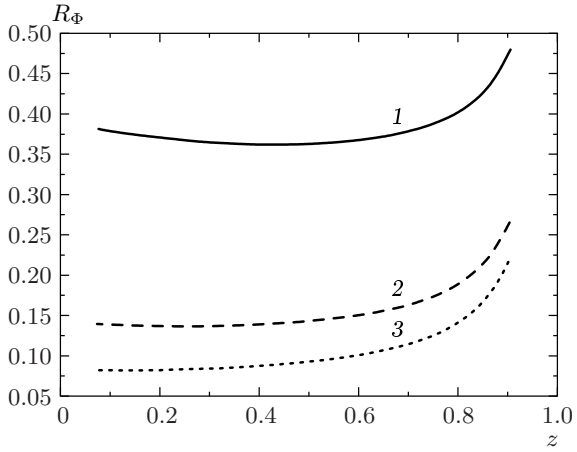

Fig. 2. The effect of a non-head-on collision of the electron and positron beams at DAΦNE is shown for the contribution of the region $D > 1$ in terms of the ratio defined by Eq. (6) at different $\theta_0 = 5^\circ$ (*1*), 10° (*2*), 15° (*3*). The approximation $4E^2(1-c_0) \gg |\mathbf{P}_\Phi|^2$ is used in calculating this ratio. The quantity R_Φ is given per cent

the corresponding cross-section can be written as [24]

$$\frac{d\sigma_0^B}{dq^2} = \frac{\alpha}{2\pi}\frac{\sigma(q^2)}{2E^2}F_0\Theta(D-1),$$

$$F_0 = \left(\frac{S}{S-q^2} - 1 + \frac{S-q^2}{2S}\right) \times$$

$$\times \left[2\ln\frac{1+c_0}{1-c_0} + \frac{|\mathbf{P}_\Phi|^2}{2E^2}\left(\ln\frac{1+c_0}{1-c_0} + \frac{c_0}{s_0^2}\right)\right] -$$

$$- \frac{S-q^2}{S}c_0\left[1 + \frac{|\mathbf{P}_\Phi|^2}{2E^2}(3-c_0^2)\right], \quad (4)$$

where $c_0 = \cos\theta_0$, $s_0 = \sin\theta_0$, and the Θ function defines the maximum possible value of q^2.

The form of F_0 and D in Eq. (4) is valid if all polar angles between θ_0 and $\pi - \theta_0$ are permitted for the tagged photon. If large-angle photons radiated between θ_l and $\pi - \theta_l$ are not recorded, we must write

$$\frac{d\sigma_l^B}{dq^2} = \frac{\alpha}{2\pi}\,\frac{\sigma(q^2)}{2E^2}(F_0 - F_l)\Theta(D_l - 1), \qquad (5)$$

where F_l can be derived from F_0 by simply replacing θ_0 with θ_l and

$$D_l = \frac{4E(E-\omega_m) - q^2 - |\mathbf{P}_\Phi|^2}{2\omega_m|\mathbf{P}_\Phi|s_l}, \quad s_l = \sin\theta_l.$$

In Sec. 3, we consider this case with $\theta_l = 40^\circ$ and call it the modified EMCAL setup.

To indicate the effect of nonzero $\mathbf{P}_\Phi$ in the first region, we show in Fig. 2 the ratio

$$R_\Phi = \frac{F_0 - F(z,c_0)}{F(z,c_0)}, \quad F(z,c_0) = F_0(\mathbf{P}_\Phi = 0) = \\ = \left[\frac{1+z^2}{1-z}\ln\frac{1+c_0}{1-c_0} - (1-z)c_0\right], \quad z = \frac{q^2}{4E^2}. \qquad (6)$$

For the modified EMCAL setup, the corresponding ratio is given by

$$R_\Phi^l = \frac{F_0 - F_l - [F(z,c_0) - F(z,c_l)]}{F(z,c_0) - F(z,c_l)}. \qquad (7)$$

As can be seen from Fig. 2, this effect does not exceed five per mille at $\theta_0 = 5^\circ$ and decreases as the angle θ_0 grows.

The contribution of the third region ($\sin\theta_0 > D > -1$) is negligible everywhere, and the second region ($1 > D > \sin\theta_0$) contributes only inside a very narrow interval of the order $2\cdot10^{-3}$ near the maximum possible di-pion invariant mass squared (see Fig. 1*b*). We therefore conclude that for restrictions (2) considered here, the effect of non-head-on collisions on the event selection at DAΦNE is about several per mille in the most important ρ resonance region and is under control where it cannot be neglected. In this region, the corresponding cross-section can therefore be given by Eq. (4) with the $F(z,c_0)$ instead of F_0 with the required accuracy.

3. VIRTUAL AND SOFT CORRECTIONS

High-precision theoretical predictions are necessary in order to reach the accuracy of one per cent in the measurement of the pion contribution to the hadronic cross-section at DAΦNE by radiative events. These predictions must at least include the first-order radiative corrections that account for the virtual and real soft photon contribution in the overall phase space and an additional contribution due to a hard photon emission inside the blind zone. In calculating radiative corrections, we neglect $\mathbf{P}_\Phi$ at the very beginning and set s, t_1, and t_2 equal to S, T_1, and T_2 at $\mathbf{P}_\Phi = 0$, respectively.

To calculate the virtual and soft corrections, we start from the corresponding expression derived in Ref. [24] (Eq. (30)), perform the trivial azimuthal angle integration, and write the result in the convenient form

$$\frac{d\sigma^{V+S}}{dq^2} = \left(\frac{\alpha}{2\pi}\right)^2\sigma(q^2)\frac{(1-z)d\cos\theta}{2s}\times \\ \times\left[\rho\frac{(q^2-t_1)^2+(q^2-t_2)^2}{t_1t_2} + T\right]\Theta(1-x_m-z), \qquad (8)$$

where

$$T = \frac{3}{2}T_g - \frac{1}{8q^2}\left[T_{11}(q^2-t_1)^2 + T_{22}(q^2-t_2)^2 + \right. \\ \left. +(T_{12}+T_{21})(sq^2 - t_1t_2)\right], \quad s = 4E^2,$$

$$\rho = 4(L_s - 1)\ln\Delta + 3L_q + \frac{2\pi^2}{3} - \frac{9}{2} + \\ + 4\left(\ln\frac{\Delta_1}{\Delta}\ln\frac{1+c_0}{1-c_0} + \ln\frac{\Delta_2}{\Delta_1}\ln\frac{1+c_1}{1-c_1}\right),$$

$$L_s = \ln\frac{s}{m^2}, \quad L_q = \ln\frac{q^2}{m^2}, \quad x_m = \frac{\omega_m}{E}.$$

The above expression for ρ contains three soft parameters Δ, Δ_1, and Δ_2. The first restricts the soft photon energy inside the blind zone with the value ΔE. It is auxiliary and cancels when the contribution caused by the hard photon emission is added (see Sec. 5). The parameters Δ_1 and Δ_2 are physical. They are defined by the sensitivity $\Delta_1 E$ of the QCAL calorimeter that surrounds the blind zone and covers polar angles of the detected photon from θ_0 to $\theta_1 = 20^\circ$ with respect to both the electron and the positron beam directions ($c_1 = \cos\theta_1$) and by the sensitivity $\Delta_2 E$ of the EMCAL calorimeter that covers the photon angles between θ_1 and $\pi - \theta_1$. The case of a slightly modified geometry of EMCAL (with the polar angles from $\theta_l = 40^\circ$ to $\pi - \theta_l$ not covered [20]) is considered in Appendix A. The coefficients T_g and T_{ik} in the right-hand side of Eq. (5) are calculated as functions of the invariants s, t_1, and t_2 in Ref. [24] (see also [29, 22]).

Our aim is to analytically integrate differential distribution (8) with respect to the tagged photon polar

angle. The integration of the term containing ρ is trivial and yields

$$\frac{d\sigma_\rho^{S+V}}{dq^2} = \left(\frac{\alpha}{2\pi}\right)^2 \frac{\sigma(q^2)}{2E^2}\rho F(z,c_0)\Theta(1-x_m-z). \quad (9)$$

To perform the remaining integrations, it is convenient to represent the quantity T as

$$\begin{aligned} T = {} & L_q^2 - L_s^2 + \frac{2s}{q^2-s} - 2L_{qs} + \left[\frac{2s(s-2q^2)}{(q^2-s)^2}+1\right]L_q + \\ & + \frac{2(2q^2-s)s}{(q^2-s)^2}L_s + L_{1q}\left[-\frac{4s^2}{(q^2-s)t_2} - \frac{2(q^4+s^2)}{(q^2-s)t_1} + 2\right] + \\ & + \ln\frac{-t_1}{m^2}\left[\frac{sq^2}{(s+t_2)^2} + \frac{q^2+3s}{s+t_2} - 1 - 2(L_q-L_s)\times\right. \\ & \left.\times\left(1-\left(\frac{2s^2}{t_2}+\frac{q^4+s^2}{t_1}\right)\frac{1}{q^2-s}\right)\right] + \\ & + \frac{2(q^4+3s^2)\left[6L_{qs}+3(L_s^2-L_q^2)+\pi^2\right]-3(q^4-2sq^2-s^2)}{6(q^2-s)t_1} - \\ & - \left[\frac{sq^2}{(s+t_1)^2} - \frac{(q^2+3s)}{s+t_1}\right]L_q - \frac{\pi^2}{3} + \\ & + \frac{s}{s+t_1} + \frac{1}{2} + (t_1 \leftrightarrow t_2), \end{aligned} \quad (10)$$

where

$$L_{qs} = \mathrm{Li}_2\left(1-\frac{q^2}{s}\right), \quad L_{1q} = \mathrm{Li}_2\left(1-\frac{t_1}{q^2}\right).$$

The Spence function L_{1q} has a nonzero imaginary part, but we must take into account only its real part in our calculations,

$$\mathrm{Re}\, L_{1q} = \frac{\pi^2}{6} - \ln\left(-\frac{t_1}{q^2}\right)\ln\left(1-\frac{t_1}{q^2}\right) - \mathrm{Li}_2\left(\frac{t_1}{q^2}\right).$$

We also note that the coefficients T_g and $T_{i,k}$ contain the terms involving $t_{1,2}^{-2}$ and $t_{1,2}^{-3}$ [22, 24, 29], but these vanish in the quantity T.

Integrating the piece of cross-section (5) that contains the quantity T with respect to the tagged photon polar angles, we obtain

$$\begin{aligned} \frac{d\sigma_T^{S+V}}{dq^2} = {} & \left(\frac{\alpha}{2\pi}\right)^2 \frac{\sigma(q^2)}{4E^2}\times \\ & \times(1-z)F_T(z,c_0)\Theta(1-x_m-z), \end{aligned} \quad (11)$$

where the function $F_T(z,c_m)$ is given in Appendix A for arbitrary values of the limiting angle θ_m. Here, we consider the case where $\theta_m = \theta_0$ and use the approximation $1-c_0 \ll 1$, which is sufficiently good for $\theta_0 \le 10^\circ$ (precisely this case is suitable for the blind zone of the KLOE detector),

$$\begin{aligned} (1-z)F_T(z,c_0\to 1) = {} & \frac{4\ln^3 z}{3(1-z)} + \\ & + \frac{2(1+z^2)}{1-z}\ln\frac{1-z}{z}\ln^2 z - (3-z)\ln\frac{(1-z)^2}{z}\ln z + \\ & + \frac{4(1-2z)}{1-z}\ln z + 4(1-z)\ln(1-z) - \\ & - 2\left[3-z-2(1+z)\ln\frac{1-z}{z}\right]\mathrm{Li}_2(1-z) + \\ & + \frac{8}{1-z}\left[\mathrm{Li}_3(1-z) + z^2\mathrm{Li}_3\left(\frac{z-1}{z}\right)\right] - \\ & - 5 + z - \frac{2(1+z^2)}{1-z}\ln z\ln^2\frac{1-c_0}{2} + \\ & + \left[1-z-\frac{2}{1-z}-\frac{2(1+z^2)}{1-z}\times\right. \\ & \left.\times\left(\ln\frac{(1-z)^2}{z}\ln z + 2\mathrm{Li}_2(1-z)\right)\right]\ln\frac{1-c_0}{2}. \end{aligned} \quad (12)$$

The total virtual and soft correction is the sum of (9) and (11).

For the modified form of the EMCAL calorimeter, the expressions for ρ and $F(z,c_0)$ in Eq. (9) and $F_T(z,c_0)$ in Eq. (11) must be changed as

$$\begin{aligned} & \rho \to \rho + 4\ln\frac{\Delta}{\Delta_2}\ln\frac{1+c_l}{1-c_l}, \\ & F(z,c_0) \to F(z,c_0) - F(z,c_l), \\ & F_T(z,c_0) \to F_T(z,c_0) - F_T(z,c_l), \end{aligned} \quad (13)$$

where the expression given in Appendix A must be used for the function $F_T(z,c_l)$ at $c_m = c_l$.

In calculating the virtual and soft corrections, we neglected terms of the order Δ_i, $i=1,2$ compared to unity. This accuracy implies the same relation between the tagged photon energy ω and the squared di-pion invariant mass q^2 as in the Born approximation,

$$\omega = E(1-z) \quad (14)$$

(provided that $\mathbf{P}_\Phi = 0$), and it suffices to guarantee the one per cent precision.

4. HARD PHOTON EMISSION INSIDE THE BLIND ZONE

Selection rules (2) used here permit the radiation of an additional invisible photon inside the blind zone. For the events

$$e^-(p_1) + e^+(p_2) \to \gamma(k_1) + \gamma(k_2) + \pi^+\pi^-(q), \quad (15)$$

one photon with the 4-momentum k_2 hits the photon detector and the other photon (with the 4-momentum k_1) is collinear and escapes it. It is obvious that relation (14) between the tagged photon energy and the squared di-pion invariant mass is violated in this case.

To calculate the corresponding contribution into radiative corrections analytically, we start with using the quasireal electron approximation for both the form of the cross-section and the underlying kinematics. Physically, this implies that we neglect terms of the order $1-c_0 \approx \theta_0^2/2$ and $m^2/E^2\theta_0^2$ compared to unity. We recall that $\theta_0^2/2 \le 0.02$ for the KLOE detector. In accordance with the quasireal electron approximation, the differential cross-section of process (15) can be written in the same form as for the inclusive (untagged photon) event selection [25],

$$d\sigma^H = 2\left(\frac{\alpha}{2\pi}\right)^2 \frac{\sigma(q^2)}{4E^2x}P(x,L_0)dx \times \times \left[\frac{(q^2-xu_1)^2+(q^2-u_2)^2}{xu_1u_2}\right] \times \times \omega_2\, d\omega_2\, dc_2\Theta(\omega_2-\omega_m), \quad (16)$$

$$P(x,L_0) = \frac{1+x^2}{1-x}L_0 - \frac{2x}{1-x},$$

$$L_0 = \ln\frac{E^2\theta_0^2}{m^2}, \quad c_2 = \cos\theta_2,$$

$$x = 1-\frac{\omega_1}{E}, \quad u_1 = -2k_2p_1, \quad u_2 = -2k_2p_2,$$

where $\omega_2(\theta_2)$ is the energy (the polar angle) of the tagged photon and ω_1 is the energy of the invisible collinear photon.

The factor $(\alpha/2\pi)P(x,L_0)dx$ describes the radiation probability of the collinear photon by the initial electron, the factor 2 accounts for the same contribution caused by the initial positron collinear radiation, and the rest is in fact the cross-section of process (1) with the reduced electron 4-momentum ($p_1 \to xp_1$) at $\mathbf{P}_\Phi = 0$.

Our aim is now to derive the differential distribution over the squared di-pion invariant mass q^2, and it is convenient to use the relation between q^2 and c_2 in order to avoid the integration over c_2 in the right-hand side of Eq. (16). To disentangle the selection rules and obtain the integration region, it is also useful to introduce the total photon energy $\Omega = \omega_1 + \omega_2$ instead of ω_2,

$$q^2 = 4E(E-\Omega) + 2\omega_1\omega_2(1-c_2), \quad dc_2 \to \frac{dq^2}{2\omega_1\omega_2}, \quad d\omega_2 \to d\Omega_2. \quad (17)$$

Taking into account that in terms of new variables,

$$u_1 = -\frac{4E^2\Omega_z}{\omega_1}, \quad u_2 = -\frac{4E}{\omega_1}[\omega_1(\Omega-\omega_1)-E\Omega_z], \quad \Omega_z = \Omega - E(1-z), \quad (18)$$

we can rewrite Eq. (16) as

$$\frac{d\sigma^H}{dq^2} = 2\left(\frac{\alpha}{2\pi}\right)^2 \frac{\sigma(q^2)}{4E^2}M(z,L_0,\omega_1,\Omega) \times \times \frac{d\omega_1 d\Omega}{E\Omega_z}\Theta(\Omega-\omega_1-\omega_m), \quad (19)$$

where

$$M(z,L_0,\omega_1,\Omega) = -L_0 - \frac{4(L_0-1)E\Omega_z}{\omega_1^2} - \frac{zE^2L_0}{(E-\omega_1)^2} + \frac{[2z-(1+z)L_0]E}{E-\omega_1} + \frac{[2(1+z^2)L_0-4z-(1-z)^2]E^2-(1-z)(\Omega-2\omega_1)E}{\omega_1(\Omega-\omega_1)-E\Omega_z}. \quad (20)$$

We note that although the term containing ω_1^2 in the denominator can be neglected in the case of the inclusive event selection [25], it is now important and even contributes to the cancellation of the auxiliary infrared parameter Δ.

We now find the integration region for the variables ω_1 and Ω determined by restrictions (2) and by the inequalities

$$-c_m < c_2 < c_m, \quad E\Delta < \omega_1 < \Omega - Ex_m \quad (21)$$

limiting the possible angles for the tagged noncollinear photon and the energies of the invisible collinear photon. Here, we do not require $1-c_m$ to be small, bearing in mind a further application to the modified EMCAL setup. The first restriction in (2) defines the maximum value of Ω; the minimum value of Ω can be obtained from relation (17) at $\omega_1 = \Delta E$ and $c_2 = c_m$,

$$\Omega_{max} = E(1-z)\left(1+\frac{\eta}{2}\right), \quad \Omega_{min} = E(1-z)\left(1+\frac{\Delta(1-c_m)}{2}\right). \quad (22)$$

The condition $c_2 > -c_m$ implies that

$$\omega^- < \omega_1 < \omega^+, \quad \omega^\pm = \frac{\Omega}{2}\left[1 \pm \sqrt{1-\frac{8E\Omega_z}{\Omega^2(1+c_m)}}\right]. \quad (23)$$

Finally, the inequality $c_2 < c_m$ can be formulated as follows: if the values of Ω are such as

$$\Omega < \Omega_c, \quad \Omega_c = E(1-z)\left(1+\frac{(1-c_m)(1-z)}{8}\right),$$

then

$$\begin{aligned} &\omega_1 > \omega_+ \quad \text{or} \quad \omega_1 < \omega_-, \\ &\omega_\pm = \frac{\Omega}{2}\left[1 \pm \sqrt{1-\frac{8E\Omega_z}{\Omega^2(1-c_m)}}\right]. \end{aligned} \tag{24}$$

The consistent combination of the set of inequalities (21)–(24) for ω_1 and Ω defines the integration region. In general, this region depends on the di-pion invariant mass through z; it is shown in Fig. 3, where we use the notation

$$\begin{aligned} &\Omega_\Delta = E(1-z)(1+\Delta), \\ &\Omega_x = E(1-z)\left[1+\frac{(1-c_0)x_m y)}{2(1-z)}\right], \\ &y = 1-z-x_m. \end{aligned} \tag{25}$$

This region differs from the corresponding region for the inclusive event selection [25].

We note that in the calculation, we controlled our analytical integration by means of the numerical one. This allowed us to conclude that in the case where

$$z < z_c = 1 - \frac{4\eta}{1-c_m},$$

the contribution of the top region in Fig. 3*a* is small, and we excluded it from consideration. Although the regions in Figs. 3*b* and *c* are different, the respective contributions to cross-section (19) have the same analytical form.

The list of the integrals that are reguired in both cases, $z < z_c$ and $z > z_c$, is given in Appendix B. Using these integrals, we write the contribution of the additional hard photon emission inside blind zone to the radiative corrections as

$$\begin{aligned} \frac{d\sigma^H}{dq^2} = &\left(\frac{\alpha}{2\pi}\right)^2 \frac{\sigma(q^2)}{2E^2} \times \\ &\times \left[G_\Delta \ln\Delta + P(z,L_0)G_p + L_0 G_1 + G_0\right]. \end{aligned} \tag{26}$$

If the tagged photon is detected in the angular region $\pi-\theta_0 > \theta > \theta_0$, the coefficients $G_i (i = \Delta, p, 1, 0)$ are given by

$$G_\Delta = 4(L_0-1)\left[1-z+\frac{1+z^2}{1-z}l_0\right], \quad l_0 = \ln\frac{\theta_0^2}{4}, \tag{27}$$

$$\begin{aligned} G_p = &-\ln^2\frac{(1-z)\eta}{2(1-z-x_m)x_m} - 2\ln\frac{1-z}{x_m} \times \\ &\times \ln\frac{4(1-z)x_m}{\eta^2} - 4\mathrm{Li}_2\left(\frac{x_m}{1-z}\right) + \pi^2 - \\ &- 2l_0 \ln\frac{(1-z)(1-z-x_m)\eta}{2x_m}, \end{aligned} \tag{28}$$

$$\begin{aligned} G_1 = x_m &\left[2+\left(1+\frac{1}{z+x_m}\right)\ln\frac{1-z}{x_m}\right] - \\ &- 2(1-z)\left(2\ln\frac{\eta}{2}+3\right) + \\ &+ (2z+x_m)\left(\frac{1}{z+x_m}-1\right) \times \\ &\times \left(l_0 + \ln\frac{2(1-z-x_m)}{\eta}\right) - (1+z) \times \\ &\times \left[\frac{1}{2}\ln^2 z - \ln z \ln\frac{x_m}{1-z} - \ln(z+x_m) \times\right. \\ &\times \left(1-l_0-\ln\frac{2x_m}{(1-z)\eta}\right) + \mathrm{Li}_2(1-z) + \\ &\left.+\mathrm{Li}_2\left(-\frac{x_m}{z}\right) - \mathrm{Li}_2(z+x_m) + \frac{\pi^2}{6}\right], \end{aligned} \tag{29}$$

$$\begin{aligned} G_0 = &-\frac{\pi^2}{3}(2-3z) + 4(1-z)\left(1+\ln\frac{\eta}{2}\right) + \\ &+ 2z\left[\frac{1}{2}\ln^2 z - \ln z \ln\frac{x_m}{1-z} + \ln(z+x_m) \times\right. \\ &\times \left(l_0 + \ln\frac{2x_m}{(1-z)\eta}\right) + \\ &\left.+ \mathrm{Li}_2(1-z) + \mathrm{Li}_2\left(-\frac{x_m}{z}\right) - \mathrm{Li}_2(z+x_m)\right] + \\ &+ (1-z)\left[\ln^2\frac{2(1-z-x_m)x_m}{(1-z)\eta} + \right. \\ &+ \ln\frac{1-z}{x_m}\ln\frac{4(1-z)x_m}{\eta^2} + 2l_0\ln\frac{(1-z-x_m)\eta}{2} + \\ &\left.+ 2\mathrm{Li}_2\left(\frac{x_m}{1-z}\right) + \mathrm{Li}_2\left(\frac{(1-z)\eta}{2(1-z-x_m)x_m}\right)\right], \end{aligned} \tag{30}$$

where we pass to the limit $1-c_0 \ll 1$ and take into account that only the regions in Figs. 3*b* and *c* contribute in this limiting case.

To describe the contribution into radiative corrections caused by the double hard photon emission with the tagged photon in the range $\pi-\theta_0 > \theta > \pi-\theta_l$, $\theta_l > \theta > \theta_0$, which corresponds to the modified EMCAL setup, we must evaluate the difference

$$\frac{d\sigma^H}{dq^2}(\theta_m = \theta_0) - \frac{d\sigma^H}{dq^2}(\theta_m = \theta_l). \tag{31}$$

We have

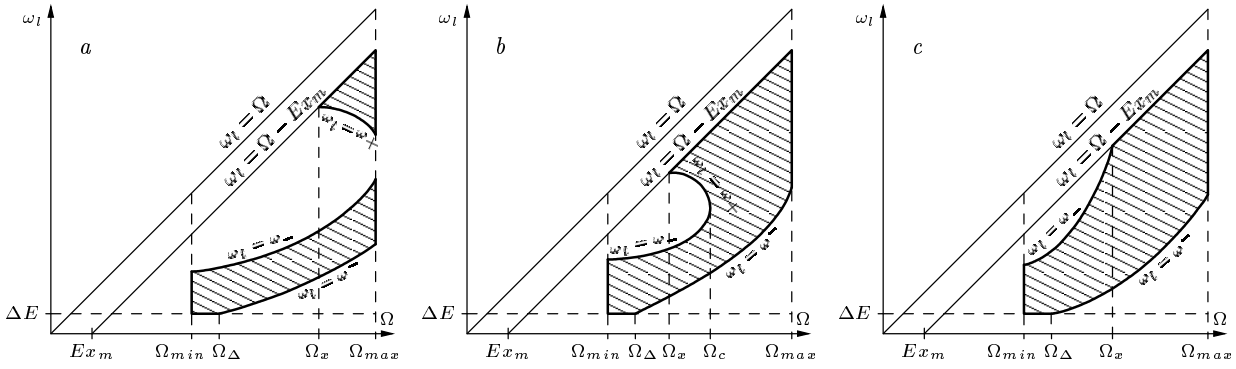

Fig. 3. The integration region for the contribution of the hard photon emission inside the blind zone in the regions $z < z_c$ (3*a*), $z_c < z < 1 - 2x_m$ (3*b*), and $1 - 2x_m < z < 1 - x_m$ (3*c*). We neglect the contribution of the top piece in Fig. 3*a*, which is justified by numerical control

$$\frac{d\sigma_M^H}{dq^2} = \left(\frac{\alpha}{2\pi}\right)^2 \frac{\sigma(q^2)}{2E^2}\left[(G_\Delta - G_\Delta^l)\ln\Delta + \right.$$
$$\left. + P(z, L_0)(G_p - G_p^l) + L_0(G_1 - G_1^l) + G_0 - G_l\right], \quad (32)$$

where the expressions for the functions G_i^l are given in Appendix C.

In this case, there also exists an additional region where the radiation of the hard photon at large angles can contribute. It covers polar angles from θ_l up to $\pi - \theta_l$. We take only one piece of the corresponding contribution into account (the one that is proportional to $\ln\Delta$) and write it as [24]

$$\frac{d\sigma_M^L}{dq^2} = \frac{d\sigma_l^B}{dq^2}\,\frac{\alpha}{2\pi} 4\ln\frac{1}{\Delta}\ln\frac{1+c_l}{1-c_l}, \quad (33)$$

where $d\sigma_l^B/dq^2$ is defined by Eq. (5). The remaining contribution is small because of restriction (2) and we expect that it is parameterically equal to $-\alpha/2\pi l_0$ relative to the Born cross-section.

5. THE TOTAL RADIATIVE CORRECTION

The total radiative correction to the cross-section of the initial-state radiation process (1) with the $\pi^+\pi^-$ hadronic final sate is defined by the sum of the contributions caused by the virtual and real soft photon emission and by the radiation of the hard collinear photon inside the blind zone of the KLOE detector. In calculating the radiative correction, we suppose that $\mathbf{P}_\Phi = 0$, because the corresponding effect due to the non-head-on collision of beams cannot be greater than 10^{-3} at the radiative correction level. It is easy to see that the auxiliary infrared cut-off parameter Δ vanishes for both forms of the EMCAL calorimeter. If $\pi - \theta_0 > \theta > \theta_0$ it enters this sum in the combination

$$\left(\frac{\alpha}{2\pi}\right)^2 \frac{\sigma(q^2)}{2E^2} \times$$
$$\times \ln\Delta\left\{\left[4(L_s - 1) + 4\ln\frac{1-c_0}{1+c_0}\right]F(z, c_0) + G_\Delta\right\}, \quad (34)$$

where the expression inside the curly brackets vanishes in the limiting case where $1 - c_0 \ll 1$, which was used in calculating G_Δ. We can therefore write the analytical expression for the derived radiative correction as

$$\frac{d\sigma^{RC}}{dq^2} = \frac{d\sigma^B}{dq^2}\delta^{RC}, \quad \delta^{RC} = \frac{\alpha}{2\pi}\,\frac{V}{F(z, c_0)}, \quad (35)$$

$$V = \tilde{\rho}F(z, c_0) + \frac{1}{2}(1 - z)F_T(z, c_0) +$$
$$+ P(z, L_0)G_p + L_0 G_1 + G_0, \quad (36)$$

where $d\sigma^B/dq^2$ is defined by Eq. (4) at $\mathbf{P}_\Phi = 0$, $\tilde{\rho}$ is ρ without the terms containing $\ln\Delta$, and the limit $1 - c_0 \ll 1$ must be taken for the functions $F(z, c_0)$ and $F_T(z, c_0)$.

For the modified EMCAL calorimeter, the expression in the curly brackets in (34) is replaced by

$$4\left\{\left[L_s - 1 + \ln\frac{(1-c_0)(1+c_l)}{(1+c_0)(1-c_l)}\right] - \right.$$
$$\left. - \ln\frac{1+c_l}{1-c_l} - L_0 + 1\right\}\left[F(z, c_0) - F(z, c_l)\right], \quad (37)$$

where the terms in the square brackets correspond to the contribution of the virtual and soft photon emission and the remaining terms are caused by the large-angle (larger than θ_l) and small-angle (smaller than θ_0) hard photon radiation.

The total radiative correction can then be written as

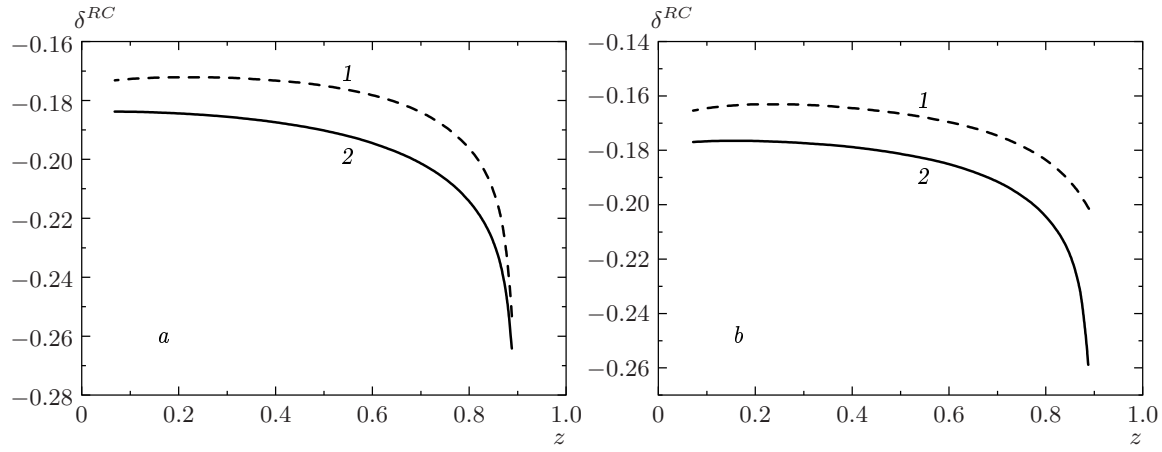

Fig. 4. Trends in the z dependence of the quantity δ^{RC} defined by Eq. (35) under the variation of the physical parameters θ_0 and x_m: a — $\theta_0 = 10^\circ$, $x_m = 0.098$ (*1*); $\theta_0 = 5^\circ$, $x_m = 0.098$ (*2*); b — $\theta_0 = 7.5^\circ$, $x_m = 0.039$ (*1*); $\theta_0 = 7.5^\circ$, $x_m = 0.098$ (*2*). All curves are calculated at $\eta = 0.02$, $\Delta_1 = 0.002$, and $\Delta_2 = 0.01$

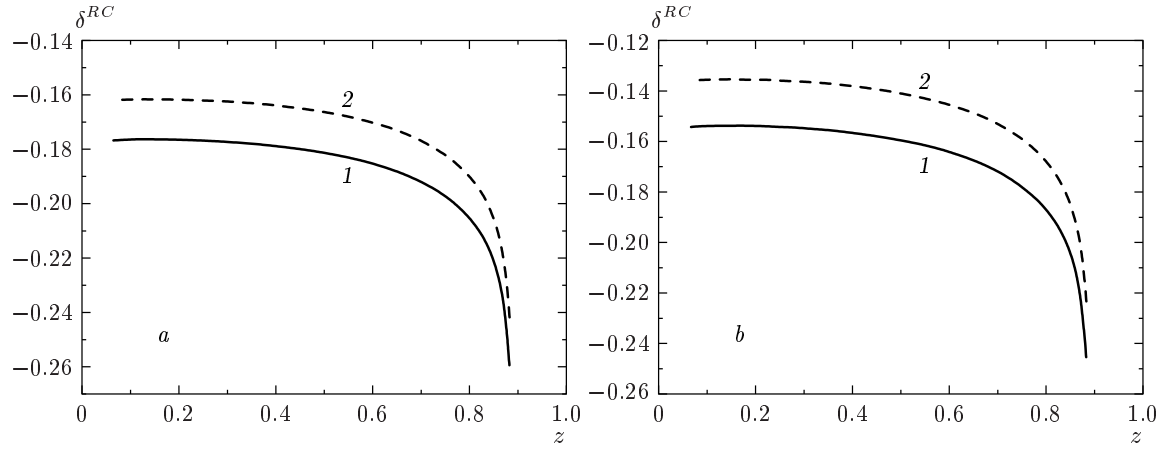

Fig. 5. Influence of the physical parameters η, Δ_1, and Δ_2 on the z dependence of δ^{RC}. The minimum energy of the tagged photon is 50 MeV ($x_m = 0.098$); a — $\theta_0 = 7.5^\circ$, $\eta = 0.02$, $\Delta_2 = 0.01$, $\Delta_1 = 0.002$ (*1*) 0.01 (*2*); b — $\theta_0 = 7.5^\circ$, $\eta = 0.03$, $\Delta_2 = 0.015$, $\Delta_1 = 0.002$ (*1*) 0.015 (*2*)

$$\delta_l^{RC} = \frac{\alpha}{2\pi}\,\frac{V_M}{[F(z,c_0) - F(z,c_l)]}, \tag{38}$$

$$V_M = \tilde{\rho}_M\,[F(z,c_0) - F(z,c_l)] + \frac{1-z}{2}\times$$
$$\times\,[F_T(z,c_0) - F_T(z,c_l)] + P(z,L_0)\,(G_p - G_p^l) +$$
$$+L_0\,(G_1 - G_1^l) + G_0 - G_0^l,$$
$$\tilde{\rho}_M = \tilde{\rho} + 4\ln\Delta_2\ln\frac{1-c_l}{1+c_l}. \tag{39}$$

To identify trends in the behavior of the radiative correction, we study its dependence on the physical parameters that define event selection rules (2), namely η and x_m, and the dependence on the opening angle of the blind zone θ_0 and the respective sensitiveness Δ_1 and Δ_2 of the QCAL and EMCAL calorimeters.

The results for δ^{RC} given by Eq. (35) are shown in Figs. 4 and 5. As was expected, the radiative correction is large and negative because the positive contribution caused by the real photon radiation cannot compensate the negative one-loop correction. This effect intensifies because the first inequality in (2) decreases the phase space of the additional invisible real photon. The absolute value of radiative correction depends on z and changes from 14 % near the $\pi^+\pi^-$ pair production threshold to 25 % at the maximum possible squared dipion invariant mass. In the more interesting region of the ρ resonance ($0.5 < z < 0.7$), it amounts to about

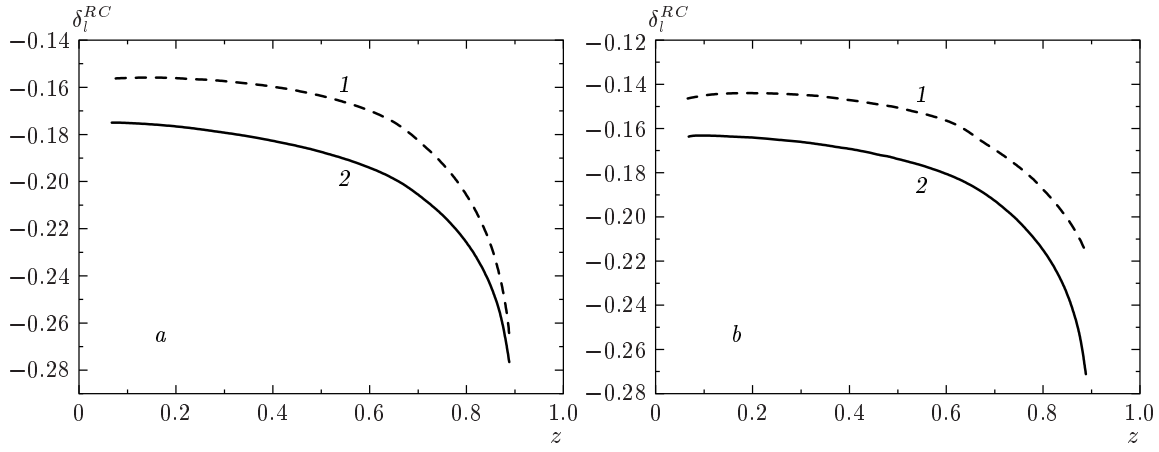

Fig. 6. The z dependence of δ_l^{RC} defined by Eq. (38) at different values of θ_0 and x_m: a — $\theta_l = 40^\circ$, $x_m = 0.098$, $\theta_0 = 10^\circ$ (*1*), 5° (*2*); b — $\theta_0 = 7.5^\circ$, $\theta_l = 40^\circ$, $x_m = 0.039$, (*1*), 0.098 (*2*)

14–20 %.

The main peculiarities in the behaviour of the radiative correction are related to the change of the positive contribution caused by the radiation of an additional invisible hard photon. If the limiting angle θ_0 decreases, the absolute value increases because the invisible photon angular phase space is then compressed. Conversely, the decrease of the minimal energy of the tagged photon leads to an expansion of the energy phase space of the invisible photon at a fixed value of Ω (see Fig. 3), and therefore, to a decrease of the absolute value. A similar effect occurs as the parameter η grows. But the total energy Ω of both the tagged and the invisible photons then increases, and the absolute value decreases as in the previous case.

The change of the parameters Δ_1 and Δ_2 affects the energy phase space of an additional real invisible soft photon inside the KLOE calorimeters. If these parameters are increased, the corresponding phase space expands and the absolute value decreases.

The total first-order radiative correction δ_l^{RC} for the modified EMCAL setup is shown in Fig. 6. Near the threshold, it is somewhat smaller than δ^{RC} in the absolute value, but it grows more rapidly with the increase of z.

Our calculations are restricted by considering only the first-order correction to the Born cross-section. But a large value of the absolute value requires evaluating the effects of higher-order QED corrections to clarify the question of whether our approximation suffices to provide the one per cent accuracy even in the region of the ρ resonance. We hope to calculate these effects elsewhere.

6. CONCLUSIONS

The radiative return method with tagged photons offers a unique opportunity for a measurement of the total hadronic cross-section $\sigma(e^+e^- \to \text{hadrons})$ over a wide range of energies. The decrease of the event number is easily compensated by a high luminosity of the new electron–positron colliders. Of a particular interest are the experimental efforts at low and intermediate energies because they are mandatory for the future of the electroweak precision physics.

Success of the precision studies of the hadronic cross-section through the measurement of radiative events relies on the matching level of reliability of the theoretical expectation. The principal problem is the analysis of radiative corrections to the initial-state radiative cross-section at realistic conditions as regards the event selection. In the present work, we have developed the approach proposed in Ref. [24] for a high-precision analytical calculation of the $e^+e^- \to \pi^+\pi^-$ channel contribution to the hadronic cross-section. This channel dominates in the range below 1 GeV because of the radiative return on the ρ resonance and the corresponding contribution can be measured with a high-precision at the DAΦNE accelerator with the multiple-purpose KLOE detector [26].

Our calculations include the analysis of the effects related to non-head-on collision of beams and the first-order radiative correction. We have demonstrated that at the Born level, the non-head-on effects do not exceed several per mille. To derive the radiative correction, we neglected this effects and also applied the quasi-real

electron method [28] to describe events with two hard photons, one tagged by the KLOE calorimeters and the other invisible inside the blind zone. This approach has allowed us to analytically disentangle realistic restrictions related to the event selection rules and the KLOE detector geometry. The first-order QED radiative correction obtained in this way is negative and large in the absolute value. We investigated the main trends in its behaviour at the variation of the physical parameters that define experimental restrictions on event selection; we conclude that the higher-order corrections must be evaluated in order to ensure the one per cent accuracy required for the theoretical predictions.

APPENDIX A

Here, we give the exact result of the analytical angular integration of the quantity T (see Eq. (8)) with respect to the tagged photon polar angles at arbitrary values of the limiting angle θ_m and the squared di-pion invariant mass,

$$\int\limits_{-c_m}^{c_m} T\,dc = 2F_T(z,c_m), \tag{A.1}$$

$$(1-z)F_T(z,c_m) = -2\frac{1+z^2}{1-z}\ln z\ln^2\frac{1-c_m}{2} + T_1(z,c_m)\ln\frac{1-c_m}{2} + T_0(z,c_m),$$

where

$$\begin{aligned}
T_0(z,c_m) = {}& \frac{4}{3(1-z)}\ln^3 z + 2c_m\left[\frac{z-5}{2} + \frac{(1-z)[-4z\ln z + ((1-c_m^2)(1-z^2)+8z)\ln(1-z)]}{[1+c_m+(1-c_m)z][1-c_m+(1+c_m)z]} + \right.\\
&\left. + \frac{3-6z+z^2}{1-z}\ln z\right] + 2[2-c_m(1-z)]\left[\left(1+\ln\frac{1+c_m}{2}\right)\ln\left(1-\frac{(1-c_m)(1-z)}{2}\right) + \right.\\
&\left. + \mathrm{Li}_2\left(-\frac{(1+c_m)(1-z)}{2z}\right)\right] - 2[2+c_m(1-z)]\times\\
&\times\left[\ln\left(1-\frac{(1+c_m)(1-z)}{2}\right)\ln\frac{1-z}{z} + \mathrm{Li}_2\left(-\frac{(1-c_m)(1-z)}{2z}\right)\right] +\\
&+ 4(1-z)c_m\mathrm{Li}_2\left(-\frac{1-z}{z}\right) + \frac{4(1+z^2)}{1-z}\ln\frac{1-z}{z}\times\\
&\times\left[\mathrm{Li}_2\left(-\frac{(1-c_m)(1-z)}{2z}\right) - \mathrm{Li}_2\left(-\frac{(1+c_m)(1-z)}{2z}\right)\right] +\\
&+ \frac{8}{1-z}\left\{2\ln z\mathrm{Li}_2\left(\frac{1-c_m}{2}\right) + \ln\frac{1-z}{z}\times\right.\\
&\times\left[\mathrm{Li}_2\left(\frac{(1-c_m)(1-z)}{2}\right) - \mathrm{Li}_2\left(\frac{(1+c_m)(1-z)}{2}\right)\right] -\\
&- z^2\left[\mathrm{Li}_3\left(-\frac{(1-c_m)(1-z)}{2z}\right) - \mathrm{Li}_3\left(-\frac{(1+c_m)(1-z)}{2z}\right)\right] -\\
&\mathrm{Li}_3\left(-\frac{1-c_m}{(1+c_m)z}\right) + \mathrm{Li}_3\left(-\frac{(1-c_m)z}{1+c_m}\right) - \mathrm{Li}_3\left(\frac{(1-c_m)(1-z)}{2}\right) + \mathrm{Li}_3\left(\frac{(1+c_m)(1-z)}{2}\right) +\\
&\left.+\frac{5+z^2}{4}\ln z\ln^2\frac{1+c_m}{2}\right\} + \frac{2}{1-z}\ln\frac{1+c_m}{2}\times\\
&\times\left\{-2z^2\ln^2 z - (3-z)(1-z)\ln z + \frac{1+2z-z^2}{2} + 2(1+z^2)\times\right.\\
&\left.\times\left[\ln z\ln(1-z) - \mathrm{Li}_2\left(-\frac{(1+c_m)(1-z)}{2z}\right)\right] +\right.\\
&\left.+ 4\mathrm{Li}_2\left(\frac{(1-c_m)(1-z)}{2}\right) + 2(1-z^2)\mathrm{Li}_2\left(-\frac{1-z}{z}\right) + (1-z)^2(1+c_m)\,\frac{3+c_m+(1-c_m)z}{1+c_m+(1-c_m)z}\right\},
\end{aligned} \tag{A.2}$$

$$T_1(z,c_m) = \frac{2}{1-z}\left\{2z^2\ln^2 z + (3-z)(1-z)\times\right.$$
$$\times\ln z - \frac{1+2z-z^2}{2} - 2(1+z^2)\times$$
$$\times\left[\ln z\ln(1-z) - \mathrm{Li}_2\left(-\frac{(1-c_m)(1-z)}{2z}\right)\right] -$$
$$-4\mathrm{Li}_2\left(\frac{(1+c_m)(1-z)}{2}\right) - 2(1-z^2)\mathrm{Li}_2\left(-\frac{1-z}{z}\right) -$$
$$-(1-z)[2+c_m(1-z)]\ln\left(1-\frac{(1+c_m)(1-z)}{2}\right) -$$
$$\left.-(1-z)^2(1-c_m)\frac{3-c_m+(1+c_m)z}{1-c_m+(1+c_m)z}\right\}. \quad \text{(A.3)}$$

We here use the standard notation for the Spence functions

$$\mathrm{Li}_2(x) = -\int\limits_0^1 \frac{dt}{t}\ln(1-xt), \quad \mathrm{Li}_3(x) = \int\limits_0^1 \frac{dt}{t}\ln t\ln(1-xt).$$

If we assume that $c_m = c_0$, $1-c_0 \ll 1$, the result in Eq. (12) is recovered.

APPENDIX B

In the case where $z > z_c$, the integration region for the double hard photon emission is shown in Figs. 3*b* and *c* and the corresponding differential cross-section is defined by Eq. (19). The list of the necessary integrals is defined by expansion (20) of the quantity $M(z, L_0, \omega_1, \Omega)$ and is given by

$$I_1 = \int \frac{d\omega_1 d\Omega}{E\Omega_z} = y\left[2 - \ln\frac{y(1-c_m)}{\eta}\right] - \\ - x_m\ln\frac{1-z}{x_m}, \quad \text{(B.1)}$$
$$y = 1 - z - x_m,$$

$$I_2 = \int \frac{d\omega_1 d\Omega}{(E-\omega_1)\Omega_z} = \frac{\pi^2}{6} + \frac{1}{2}\ln^2 z + \\ + \ln(z+x_m)\ln\frac{(1-c_m)x_m}{\eta(1-z)} + \ln z\ln\frac{1-z}{x_m} + \\ + \mathrm{Li}_2\left(-\frac{x_m}{z}\right) + \mathrm{Li}_2(1-z) - \mathrm{Li}_2(z+x_m), \quad \text{(B.2)}$$

$$I_3 = \int \frac{E\, d\omega_1 d\Omega}{(E-\omega_1)^2\Omega_z} = -\frac{x_m}{z(z+x_m)}\ln\frac{1-z}{x_m} - \\ - \frac{1+z}{z}\ln(z+x_m) - \frac{y}{z+x_m}\ln\frac{(1-c_m)y}{\eta}, \quad \text{(B.3)}$$

$$I_4 = \int \frac{(\Omega-2\omega_1)d\omega_1 d\Omega}{[\omega_1(\Omega-\omega_1) - E\Omega_z]\Omega_z} = \\ = \frac{\pi^2}{6} - \frac{1}{2}\ln^2\frac{1+c_m}{2} - \\ - \ln\frac{1-c_m}{1+c_m}\ln\frac{x_m y\eta}{2(1-z)\Delta^2} - \\ - \frac{1}{2}\ln^2\frac{2x_m y}{(1-z)\eta} - \mathrm{Li}_2\left(\frac{1-c_m}{2}\right) - \\ - \mathrm{Li}_2\left(\frac{(1-z)\eta}{2x_m y}\right), \quad \text{(B.4)}$$

$$I_5 = \int \frac{(1-z)E\; d\omega_1 d\Omega}{[\omega_1(\Omega-\omega_1) - E\Omega_z]\Omega_z} = \\ = \frac{\pi^2}{2} - \frac{4y}{1-z} - 2\mathrm{Li}_2\left(\frac{x_m}{1-z}\right) - \\ - \frac{2(1+c_m)}{1-c_m}\left[\ln\frac{1+c_m}{2} - \ln\left(\frac{2}{1-c_m} - \frac{x_m}{1-z}\right) + \right. \\ \left. + \ln\left(\frac{1+c_m}{1-c_m} + \frac{x_m}{1-z}\right)\right] + \\ + \ln\frac{1-c_m}{1+c_m}\ln\frac{2\Delta^2 x_m}{y(1-z)\eta} - \frac{1}{2}\ln^2\frac{2y}{\eta} - \\ - \frac{3}{2}\ln^2\frac{1-z}{x_m} + \ln\frac{1-x}{x_m}\ln\frac{y\eta}{2x_m^2} + \\ + \mathrm{Li}_2\left(\frac{y(1-c_m)}{2(1-z)}\right) - \mathrm{Li}_2\left(-\frac{y(1-c_m)}{(1+c_m)(1-z)}\right) + \\ + \mathrm{Li}_2\left(-\frac{x_m(1-c_m)}{(1+c_m)(1-z)}\right) - \mathrm{Li}_2\left(\frac{x_m(1-c_m)}{2(1-z)}\right), \quad \text{(B.5)}$$

$$I_6 = \int \frac{d\omega_1 d\Omega}{\omega_1^2} = \frac{(1-z)}{2}\times \\ \times\left[2(1-c_m\ln\Delta) - (1+c_m)\ln\frac{1+c_m}{\eta} - \right. \\ \left. - (1-c_m)\left(\ln y + \frac{x_m}{1-z}\right)\right]. \quad \text{(B.6)}$$

In calculating these integrals, we neglected terms of the order x_m^2 and $(1-c_m)x_m$ compared to unity; these terms are of the same order as the parameter η.

In the cases where

$$z < 1 - \frac{4\eta}{1-c_m},$$

we must integrate over the region shown in Fig. 3*a*. As mentioned above, the contribution of the top piece of this region, where

$$\Omega - Ex_m > \omega_1 > \omega^+,$$

is small (about 1–2 %) compared to the bottom one and can be neglected. This approximation is sufficient to provide the one per cent accuracy of radiative

correction. We use the notation J_i, similarly to I_i, to label separate integrals over this region,

$$J_1 = I_1 + L_K - 2(K_+ - K_-),$$
$$K_\pm = \frac{1}{2}\left(1 \pm \sqrt{1 - \frac{4\eta}{(1-c_m)(1-z)}}\right), \qquad \text{(B.7)}$$
$$L_K = \ln\frac{K_+}{K_-},$$

$$J_2 = I_2 - \ln z L_K + \mathrm{Li}_2((1-z)K_-) - \mathrm{Li}_2((1-z)K_+) -$$
$$- \mathrm{Li}_2\left(-\frac{(1-z)K_-}{z}\right) + \mathrm{Li}_2\left(-\frac{(1-z)K_+}{z}\right), \qquad \text{(B.8)}$$

$$J_3 = I_3 + \frac{1-z}{z}L_K - \frac{1+z}{z}\ln\frac{z+(1-z)K_+}{z+(1-z)K_-}, \qquad \text{(B.9)}$$

$$J_4 = I_4 + \ln\frac{1-c_m}{2}\left(\ln\frac{1-c_m}{2} - \frac{1}{2}\ln\frac{1-c_m}{1+c_m}\right), \qquad \text{(B.10)}$$

$$J_5 = 2\ln\frac{1-c_m}{1+c_m}\ln\Delta + \frac{\pi^2}{6} + 2\mathrm{Li}_2(K_-) - 4K_- +$$
$$+ \frac{1}{2}\ln^2\frac{1-c_m}{1+c_m} - 2\ln(1-z)\ln\frac{1-c_m}{1+c_m} -$$
$$- \frac{1}{2}\ln^2\frac{(1-c_m)\eta}{2(1+c_m)(1-z)} -$$
$$- \frac{1}{2}\ln\frac{(1+c_m)^2\eta}{4(1-c_m)(1-z)}L_K + \ln K_-\ln K_+ +$$
$$+ \frac{2(1+c_m)}{1-c_m}\ln\frac{2(1+c_m+(1-c_m)K_-)}{(1+c_m)(1+c_m+(1-c_m)K_+)} +$$
$$+ \mathrm{Li}_2\left(-\frac{(1-c_m)K_+}{1+c_m}\right) -$$
$$- \mathrm{Li}_2\left(-\frac{(1-c_m)K_-}{1+c_m}\right) + \mathrm{Li}_2\left(-\frac{(1-c_m)K_-}{2}\right) -$$
$$- \mathrm{Li}_2\left(-\frac{(1-c_m)K_+}{2}\right), \qquad \text{(B.11)}$$

$$J_6 = I_6 + \frac{(1-z)(1-c_m)}{2}\left(\ln\frac{(1-z)(1-c_m)}{\eta} - \right.$$
$$\left. - \frac{x_m}{1-z} - 2\ln K_+ - 2(K_+ - K_-)\right). \qquad \text{(B.12)}$$

APPENDIX C

In this Appendix, we give the analytical form of the functions G_i^l for arbitrary values of the limiting tagged photon angle θ_l. The only condition on θ_l used in Appendix B is that

$$(1-c_l)x_m \ll 1.$$

This restricts θ_l by the values about 45°. With the exception of G_Δ^l, the functions G_i^l are different for $z > z_c$ and $z < z_c$. In the first case, we have

$$G_\Delta^l(z > z_c) = 4(L_0 - 1)\left[c_l(1-z) + \frac{1+z^2}{1-z}\ln\frac{1-c_l}{1+c_l}\right]\ln\Delta, \qquad \text{(C.1)}$$

$$G_p^l(z > z_c) = -2\ln\frac{1-c_l}{1+c_l}\ln\frac{(1-z)y\eta}{2x_m} - \ln^2\frac{x_m\eta}{2(1-z)y} - 2\ln\frac{1-z}{x_m}\ln\frac{(1-z)x_m}{y^2} + \pi^2 - \frac{8y}{1-z} -$$
$$- \frac{4(1+c_l)}{1-c_l}\ln\frac{(1+c_l)[(1-c_l)(1-z)+x_m(1-c_l)]}{2[2(1-z)-x_m(1-c_l)]} - 4\mathrm{Li}_2\left(\frac{x_m}{1-z}\right) + 2\mathrm{Li}_2\left(\frac{(1-c_l)y}{2(1-z)}\right) -$$
$$- 2\mathrm{Li}_2\left(\frac{(1-c_l)x_m}{2(1-z)}\right) + 2\mathrm{Li}_2\left(-\frac{(1-c_l)x_m}{(1+c_l)(1-z)}\right) - 2\mathrm{Li}_2\left(\frac{(1-c_l)y}{(1+c_l)(1-z)}\right), \qquad \text{(C.2)}$$

$$G_1^l(z > z_c) = x_m\left(2(2-c_l) + \frac{1+z+x_m}{z+x_m}\ln\frac{1-z}{x_m}\right) + 2(1-z)\left[(1-c_l)\ln y - (1+c_l)\ln\frac{1+c_l}{\eta} - 3\right] +$$
$$+ \frac{y(2z+x_m)}{z+x_m}\ln\frac{(1-c_l)y}{\eta} + (1+z)\left[\ln\frac{1-z}{x_m}\ln\frac{z+x_m}{z} + \ln(z+x_m)\left(1 - \ln\frac{1-c_l}{\eta}\right) + \right.$$
$$\left. + \mathrm{Li}_2\left(\frac{z-1}{z}\right) - \mathrm{Li}_2\left(\frac{-x_m}{z}\right) + \mathrm{Li}_2(z+x_m) - \frac{\pi^2}{6}\right], \qquad \text{(C.3)}$$

$$G_0^l(z>z_c) = \frac{\pi^2}{3}(3z-2) - 2x_m(3-c_l) - 2z\left[\ln\frac{1-z}{x_m}\ln\frac{z+x_m}{z} - \ln(z+x_m)\ln\frac{1-c_l}{\eta} - \right.$$
$$\left. -\mathrm{Li}_2\left(\frac{z-1}{z}\right) + \mathrm{Li}_2\left(\frac{-x_m}{z}\right) + \mathrm{Li}_2(z+x_m)\right] + (1-z)\left[8 + \frac{1}{2}\ln^2\frac{1+c_l}{2} - \ln^2\frac{1-c_l}{1+c_l} + \right.$$
$$+ \ln^2\frac{(1-c_l)\eta}{2(1+c_l)y} + 4y\ln\frac{1-c_l}{1+c_l} + 2\ln\frac{1-z}{x_m}\ln\frac{1-z}{y} - 2(1-c_l)\ln y + \mathrm{Li}_2\left(\frac{1-c_l}{2}\right) + 2\mathrm{Li}_2\left(\frac{x_m}{1-z}\right) +$$
$$+ \mathrm{Li}_2\left(\frac{(1-z)\eta}{2yx_m}\right) + \mathrm{Li}_2\left(\frac{(1-c_l)x_m}{2(1-z)}\right) - \mathrm{Li}_2\left(\frac{(1-c_l)y}{2(1-z)}\right) - \mathrm{Li}_2\left(-\frac{(1-c_l)x_m}{(1+c_l)(1-z)}\right) +$$
$$\left. +\mathrm{Li}_2\left(-\frac{(1-c_l)y}{(1+c_l)(1-z)}\right) + 2\frac{1+c_l}{1-c_l}\left(\ln\frac{(1+c_l)[(1-c_l)(1-z)+x_m(1-c_l)]}{2[2(1-z)-x_m(1-c_l)]} - \ln\frac{1+c_l}{\eta}\right)\right]. \quad \text{(C.4)}$$

In the case where $z < z_c$, the corresponding functions G_i^l are given by

$$G_p^l(z<z_c) = \frac{\pi^2}{3} - 8K_- - \ln^2\frac{\eta}{2(1-z)} - 2\ln\frac{1-c_l}{1+c_l}\ln\frac{\eta(1-z)}{2} + 2\ln K_+\ln K_- -$$
$$- \ln\frac{(1+c_l)^2\eta}{4(1-c_l)(1-z)}L_K + \frac{4(1+c_l)}{1-c_l}\ln\frac{2[1+c_l+(1-c_l)K_-]}{(1+c_l)[1+c_l+(1-c_l)K_+]} + 2\mathrm{Li}_2\left(\frac{(1-c_l)K_-}{2}\right) -$$
$$- 4\mathrm{Li}_2(K_-) - 2\mathrm{Li}_2\left(\frac{(1-c_l)K_+}{2}\right) + 2\mathrm{Li}_2\left(-\frac{(1-c_l)K_+}{1+c_l}\right) - 2\mathrm{Li}_2\left(-\frac{(1-c_l)K_-}{1+c_l}\right), \quad \text{(C.5)}$$

$$G_1^l(z<z_c) = 2x_m(3-2c_l) + \frac{2-y}{1-y}\left[x_m\ln\frac{1-z}{x_m} + y\ln\frac{y(1-c_l)}{\eta}\right] +$$
$$+ 2(1-z)\left[(3-2c_l)(K_+-K_-) - 3 - (2-c_l)L_K + (1-c_l)\ln y + (1+c_l)\ln\frac{1+c_l}{\eta}\right] +$$
$$+ (1+z)\left[-\frac{\pi^2}{6} + \left(1+\ln\frac{(1-z)\eta}{(1-c_l)x_m}\right)\ln(z+x_m) + \ln z\left(L_k - \ln\frac{1-z}{x_m}\right) + \ln\frac{z+(1-z)K_+}{z+(1-z)K_-} + \right.$$
$$+ \mathrm{Li}_2\left(\frac{z-1}{z}\right) + \mathrm{Li}_2(z+x_m) - \mathrm{Li}_2\left(-\frac{x_m}{z}\right) +$$
$$\left. + \mathrm{Li}_2\left(\frac{(z-1)K_-}{z}\right) - \mathrm{Li}_2\left(\frac{(z-1)K_-}{z}\right) + \mathrm{Li}_2((1-z)K_+) - \mathrm{Li}_2((1-z)K_-)\right], \quad \text{(C.6)}$$

$$G_0^l(z<z_c) = -4x_m(1-c_l) + (1-z)\left[6 - \frac{\pi^2}{3} - 2(3-2c_l)(K_+-K_-) + \frac{1}{2}\ln^2\frac{(1-z)^2}{yx_m} - \right.$$
$$- 2(1-c_l)\ln y - 2(1+c_l)\ln\frac{1+c_l}{\eta} + \ln^2\frac{1-c_l}{2} - 2\ln\frac{1-c_l}{1+c_l}\ln\frac{1-c_l}{2yx_m} + \ln^2\frac{2(1-z)(1+c_l)}{\eta(1-c_l)} +$$
$$+ \left(2(1-c_l) + \frac{1}{2}\ln\frac{(1+c_l)^2\eta}{4(1-c_l)(1-z)}\right)L_K - \ln K_+\ln K_- - \ln\frac{(1-z)^2}{yx_m}\ln\frac{2(1+c_l)(1-z)}{(1-c_l)\eta} -$$
$$- 2\mathrm{Li}_2(K_-) - \mathrm{Li}_2\left(\frac{(1-c_l)K_-}{2}\right) + \mathrm{Li}_2\left(\frac{(1-c_l)K_+}{2}\right) + \mathrm{Li}_2\left(-\frac{(1-c_l)K_-}{(1+c_l)}\right) - \mathrm{Li}_2\left(-\frac{(1-c_l)K_+}{1+c_l}\right) +$$
$$+ \mathrm{Li}_2\left(\frac{1-c_l}{2}\right) + \mathrm{Li}_2\left(\frac{(1-z)\eta}{2yx_m}\right) + \frac{2(1+c_l)}{1-c_l}\ln\frac{(1+c_l)[1+c_l+(1-c_l)K_+]}{2[1+c_l+(1-c_l)K_-]}\Bigg] +$$
$$+ 2z\left[\frac{\pi^2}{6} + \ln\frac{(1-c_l)x_m}{(1-z)\eta}\ln(z+x_m) - \ln z\left(L_K - \ln\frac{1-z}{x_m}\right) + \right.$$
$$+ \mathrm{Li}_2\left(-\frac{x_m}{z}\right) - \mathrm{Li}_2\left(\frac{z-1}{z}\right) - \mathrm{Li}_2(z+x_m) + \mathrm{Li}_2((1-z)K_-) - \mathrm{Li}_2((1-z)K_+) +$$
$$\left. + \mathrm{Li}_2\left(\frac{(z-1)K_+}{z}\right) - \mathrm{Li}_2\left(\frac{(z-1)K_+}{z}\right)\right]. \quad \text{(C.7)}$$

REFERENCES

1. R. M. Carey et al., (g-2) Collaboration, Phys. Rev. Lett. **82**, 1632 (1999); H. M. Brown et al., (g-2) Collaboration, Phys. Rev. D **62**, 0901101 (2000); Phys. Rev. Lett. **86**, 2227 (2000); B. Lee Roberts et al., (g-2) Collaboration, E-print archives hep-ex/0111046.

2. A. H. Hőcker, E-print archives hep-ph/0111243; J. F. de Trocóniz and F. J. Yndurain, E-print archives hep-ph/0111258.

3. V. M. Hugles and T. Kinoshita, Rev. Mod. Phys. **71**, 133 (1999).

4. S. Peris, M. Perrottet and E. de Rafael, Phys. Lett. B **355**, 523 (1995); A. Czarneski, B. Krause, and W. J. Marciano, Phys. Rev. D **52**, R2619 (1995); E. A. Kuraev, T. V. Kuchto, and A. Shiller, Yad. Fiz. **51**, 1631 (1990); E. A. Kuraev, T. V. Kuchto, Z. K. Silagadze, and A. Shiller, Preprint, INP 90-66, Novosibirsk (1990).

5. M. Knecht and A. Nyffeler, E-print archives hep-ph/0111058; M. Knecht, A. Nyffeler, M. Perrottet, and E. de Rafael, E-print archives hep-ph/0111059.

6. J. Bijnens, E. Pallante, and J. Prades, Phys. Rev. Lett. **75**, 3784 (1995), Nucl. Phys. B **474**, 379 (1996).

7. M. Hayakawa, T. Kinoshita, and A. I. Sanda, Phys. Rev. Lett. **75**, 790 (1995), Phys. Rev. D **54**, 3137 (1996); M. Hayakawa and T. Kinoshita, Phys. Rev. D **57**, 465 (1998).

8. J. Bijnens, E. Pallante, and J. Prades, Preprint LUTP 01-37, E-print archives hep-ph/0112255.

9. M. Hayakawa and T. Kinoshita, Preprint KEK-TH-993, E-print archives hep-ph/0112102.

10. N. Cabibbo and R. Gatto, Phys. Rev. **124**, 1577 (1961); M. Gourdin and E. de Rafael, Nucl. Phys. B **10**, 667 (1967).

11. A. Charnecki and W. J. Marciano, E-print archives hep-ph/0102122; W. J. Marchiano and B. L. Roberts, E-print archives hep-ph/0105056; K. Melnikov, SLUC-PUB-8844, E-print archives hep-ph/0105267; F. J. Yndurain, E-print archives hep-ph/0103212; F. Jegerlehner, E-print archives hep-ph/0001386.

12. M. Davier and H. Hőcker, Phys. Lett. B **419**, 419 (1998), **435**, 427 (1998).

13. S. Narison, Phys. Lett. B **513**, 53 (2001); V. Cirigliano, G. Ecker, and H. Neufeld, Phys. Lett. B **513**, 361 (2001).

14. J. F. Trocóniz and F. J. Yndurain, E-print archives hep-ph/0106025; J. Prades, E-print archives hep-ph/0108192.

15. R. R. Akhmetshin et al., E-print archives hep-ex/9904027; Nucl. Phys. A **675**, 424 (2000); Phys. Lett. B **475**, 190 (2000).

16. D. Kong, E-print archives hep-ph/9903521: J. Z. Bai et al., BES Collaboration, Phys. Rev. Lett. **84**, 594 (2000); E-print archives hep-ph/0102003.

17. F. Jegerlehner, E-print archives hep-ph/0104304, E-print archives hep-ph/0105283.

18. A. B. Arbuzov et al., JHEP 12 (1998) 009; M. Konchatnij and N. P. Merenkov, JETP Lett. **69**, 811 (1999).

19. S. Binner, J. H. Kűhn, and K. Melnikov, Phys. Lett. B **459**, 279 (1999); K. Melnikov et al., Phys. Lett. B **477**, 114 (2000); H. Czyź and J. H. Kűhn, Eur. Phys. J. C **18**, 497 (2001).

20. S. Spagnolo, Eur. Phys. J. C **6**, 637 (1999); G. Cataldi et al., KLOE MEMO 195, August 13, 1999.

21. A. Hoefer, J. Gluza, F. Jegerlehner, E-print archives hep-ph/0107154.

22. G. Rodrigo et al., Eur. Phys. J. C **22**, 81 (2001), E-print archives hep-ph/0106132; G. Rodrigo, E-print archives hep-ph/0111151; G. Rodrigo et al., E-print archives hep-ph/0112184.

23. G. Cataldi et al., Physics and Detectors at DAΦNE, 569 (1999).

24. V. A. Khoze et al., Eur. Phys. J. C **18**, 481 (2001).

25. N. P. Merenkov and O. N. Shekhovtsova, Pis'ma Zh. Exs. Teor. Fiz. **74**, 69 (2001); V. A. Khoze et al., E-print archives hep-ph/0202021 (submitted to Eur. Phys. J. C).

26. M. Adinolfi et al., KLOE Collaboration, E-print archives hep-ex/0006036; A. Aloisio et al., KLOE Collaboration, E-print archives hep-ex/0107023; A. Denig (on behalf of KLOE Collaboration), E-print archives hep-ex/0106100.

27. E. P. Solodov (BABAR Collaboration), E-print archives hep-ex/0107027.

28. V. N. Baier, V. S. Fadin, and V. A. Khoze, Nucl. Phys. B **65**, 381 (1973).

29. E. A. Kuraev, N. P. Merenkov, and V. S. Fadin, Sov. J. Nucl. Phys. **45**, 486 (1987).